Royal Norwegian Council
for Scientific and Industrial Research
(NTNF)

NORSAR

NORSAR Scientific Report No. 1-92/93

Semiannual Technical Summary

1 April — 30 September 1992

Kjeller, November 1992

7.5 Initial results from global Generalized Beamforming

We will in this paper outline some of the fundamental concepts for using the Generalized BeamForming method (GBF) to conduct phase association and event location on a global scale. Towards the end of the paper we will also present initial results from GBF processing of detection data from the GSETT-2 database. The GSETT-2 network consisted of about 60 globally distributed stations (including single-component, three-component and arrays), see Fig. 7.3.2., which reported phase readings and waveforms to a common database during a period of six weeks. Detailed instructions for the conduct of the GSETT-2 experiment are given in GSE/CRP190/Rev.4 (1991).

The Generalized Beamforming method for phase association and event location (Ringdal and Kværna, 1989), has been proven to work well on a regional scale (distances within approximately 2000 km) using continuous detection data from the four regional arrays ARCESS, FINESA, GERESS and NORESS (Kværna, 1990; Kværna, 1992). Taylor and Leonard (1992) are currently conducting research on applying this method to teleseismic data from a 17 station global network. Their results indicate that the GBF method can be effectively used as a means of conducting automatic global teleseismic phase association.

In order to extend the GBF method to work on both regional and teleseismic data from a large global network we have found it necessary to develop a framework that facilitates testing of the method with different parameter settings. We will in the following give a detailed description of this framework.

Division of the earth into regular target regions

The basic idea behind the GBF method is to match the predicted phase arrivals from hypothetical events in a predefined set of target regions to the actual detections at each observing station. We have chosen to define these target regions by their center coordinates and a circular area of a given radius. Initially we will deploy the center of the target regions at a common depth and ensure that the circular areas cover the entire surface of the earth. In practice, the target region will constitute a volume around the center grid point, and will thus also accommodate hypothetical events within a given depth range.

In section 7.4, we have described two techniques for constructing a uniform grid system covering the earth's surface. Results from this study indicate that the method based on triangulation of the icosaeder (the triangular method) is preferable. The density of the grid system is given by a single variable determining how many times the original icosaeder is divided by triangulation. Figs. 7.5.1 - 7.5.3 show global grid systems obtained by two-, three- and four-fold triangulation of the icosaeder. The number of global grid points in these figures are respectively 162, 642 and 2562, and the respective radii of the corresponding circular areas encompassing each grid point are 11.0, 5.5 and 2.7 degrees.

Parameter tolerances due to the areal extent of the target region

Time tolerances

On the global map of Fig. 7.5.4 we have plotted a 162-point global grid system with target regions of 11 degrees radii. Let us consider a P-phase at the NORESS array from a hypothetical event in the highlighted target region. As shown on Fig. 7.5.5, the P-phase travel-times from events within this target region can differ by almost 200 seconds. This has to be taken into account in the process of matching predicted and observed phase arrivals, and in practice, the following procedure is used:

Assume that we have a phase detection at the NORESS array with arrival time T_{arr}. The minimum and maximum predicted travel-times of P-phases from the highlighted target region are given by TT_{min} and TT_{max}. If the observed arrival at NORESS is to be a P-phase from an event in the target region, the origin time of the event would theoretically be bounded by OT_{min} and OT_{max} given by

$$OT_{min} = T_{arr} - TT_{max} \quad (1)$$

$$OT_{max} = T_{arr} - TT_{min} \quad (2)$$

Slowness vector tolerances

If the observing station is providing azimuth and/or slowness estimates of the detected phases, these estimates can constrain the use of the detections in the phase association process, and thus prevent false associations. Let us again consider a P-phase at the NORESS array from a hypothetical event in the highlighted target region shown on Fig. 7.5.4. To cover the entire target region, the P-phases will theoretically span an azimuth and slowness range falling within the solid curve of Fig. 7.5.6. In practice, we make an approximation to the area within the solid curve by specifying four parameters, i.e., the minimum and maximum values of slowness and azimuth. As seen on Fig. 7.5.6, this will constitute an area only marginally larger than the original. So in order to match the observed arrival at NORESS to a P-phase from a hypothetical event in the target region, the estimated azimuth and slowness would theoretically have to fall within these bounds.

Parameter tolerances due to deviations from the theoretical model

Time tolerances

In addition to the parameter tolerances compensating for the areal extent of the source region, we also have to take into account the effects of sampling rate, errors in the estimation of arrival-time and slowness vector, propagation path, source type and other types of random errors.

Let ΔT be the sampling rate in time of the generalized beam for the highlighted target region of Fig. 7.5.4, and let T_{dev-} (early arrival) and T_{dev+} (late arrival) be the maximum allowable deviations from the predicted P travel-time, taking into account path

effects, onset time estimation errors, source effects and other types of random errors. If we again consider the situation with a phase detection at the NORESS array with arrival time T_{arr}, hypothesized to be a P-phase from an event in the highlighted target region, we find that the origin time of the event has to be within the following bounds:

$$OT_{low} = T_{arr} - TT_{max} - \frac{\Delta T}{2} - T_{dev-} \quad (3)$$

$$OT_{high} = T_{arr} - TT_{min} + \frac{\Delta T}{2} + T_{dev+} \quad (4)$$

These are the bounds actually used in the GBF matching procedure. Initial residual requirements (T_{dev-} and T_{dev+}) for P-phases in the GSETT-2 experiment were 1.5 seconds, whereas for S-phases they were set to 7.5 seconds.

Slowness vector tolerances

One way of including the effects of random errors when matching the estimated and predicted slowness vectors, is to require the absolute value of the slowness vector residual to be less than a predefined value. In the GSETT-2 experiment different requirements were used for three-component stations, high-frequency arrays and short-period arrays, reflecting their different abilities to correctly estimate the slowness vector.

The procedure of comparing a slowness vector observation with the predicted slowness and azimuth range of a target region, including the residual requirement, can be described by the following example:

Let us again consider the situation of a P-phase at the NORESS array from a hypothetical event in the highlighted target region of Fig. 7.5.4. A phase detection at NORESS has a slowness and azimuth estimate given by the asterisk on Fig. 7.5.7, and according to the GSETT-2 instructions, the corresponding residual requirement is 3.0 sec/deg, indicated by the circular area encompassing the estimated slowness vector. If there is an overlap between this circular area and the sector segment corresponding to the expected range of slowness vectors from the target region (also see Fig. 7.5.6), the phase detection is said to match the P-phase of a hypothetical event in the actual target region. On the other hand, if there is no overlap, the observation is not matching this hypothesis.

Additional constraints on the use of a phase detection

When initiating the GBF procedure with a predefined set of target regions, we compute and store the minimum and maximum azimuths and distances to every station in the network. The availability of these parameters enables us to constrain the use of a phase detection in a simple and well-organized way.

As an example, assume that we have a phase detection with peak frequency well above 10 Hz, and that we are trying to match this detection to an Lg phase from a hypothetical event in a target region located 15-20 degrees away from the recording station. Accumulated statistics has shown that at this station, Lg with peak frequencies above 10 Hz are

never observed from events at distances greater than 5 degrees. As such information is easily included in the data structure of the GBF procedure, we can compare this information to the actual distance to the target region, and consequently find that this phase detection cannot be an Lg phase originating in this target region.

Another example: A P and an S-phase recorded at an array station have been associated and an initial event location has been provided. Accumulated event statistics at this station has given us an estimate of the uncertainty of such one-array event locations. If a target region is located too far away from the one-array event location, these two phases can be excluded as originating from an event in this target region.

A third example: Several successive phase detections at a given station have been associated with the same event, either by automatic processing or by an analyst. If we are matching these detections to an event in a target region from where Pn is expected to be the first-arriving phase, only the first of the consecutive detections can possibly be the Pn-phase (we ignore multiple events at this stage). Such context-dependent information is straightforward to include in the GBF algorithm.

These three examples constitute samples from three different classes of constraints that can be imposed on the use of a phase detection.

- Constraints inferred from measurements on a single phase, e.g., slowness vector, dominant frequency, frequency spectrum, polarization attributes, signal-to-noise ratios, etc.
- Constraints inferred from a reported event location at a given station.
- Constraints inferred from the pattern of detections at a given station. The last two types of constraints are based on so-called context-dependent information.

Step-by-step description of the GBF method

Having defined some of the key elements of the GBF method for phase association and event location, we will continue with a step-by-step description of the algorithm.

- **Definition of the station network**: Determine which stations to process for phase association and event location.
- **Definition of initial phase type candidates**: Decide the phase types that may be considered in the phase matching process, e.g. P, PKP, Pn, Pg, S, Sn, Lg, Rg, etc.
- **Constraining the use of the phase detections**: From phase measurements (dominant frequency, slowness, azimuth, etc.), single station location reports and other single-station context information, we do, for every phase detection at every station, impose constraints on their use. For each initial phase type candidate, every detection is assigned a row in a database table. This row may contain information on the allowable distance range, depth range, and azimuth range of a hypothetical event creating this hypothetical phase type. If no constraints are imposed, the distance range is set to 0-180 degrees, the depth range to 0-1000 km and the azimuth range to

± 180 degrees. If it is determined that a detection does not correspond to one of the initial phase-type candidates, e.g. Rg, the distance range of the Rg-row is set to a negative value.

- **Construct a grid of target regions**: By using the triangular method, a global grid system of a predefined density is constructed, see section 7.4.
- **Determine which of the initial phase type candidates to consider**: For every station-target region combination, we decide which of the initial phase type candidates to consider for phase matching. E.g., if a target region is located 60-70 degrees away from a station, it makes no sense to use regional phases like Pn, Pg, Sn, Lg or Rg. On the other hand, if a target region is located at regional distances from a station, teleseismic phases for that station can be ignored. Along with the list of phases to consider from each target region, we store the expected travel-times, slownesses and azimuths, as well as the respective tolerance limits. The decision of which phases to consider and their corresponding travel-times and slowness vectors can be inferred from general travel-time tables and great-circle azimuths, or, if available, from regional knowledge on the wave propagation characteristics at a given station, see section 7.3.
- **Compute generalized beams for each target region**: For each target region, at regular origin time intervals, we match the observed phase detections in the network to the predicted phase arrivals from a hypothetical event in the region. The value of the generalized beam at a given origin time is the actual number of matching phase detections. To avoid a list of phase associations that may look unreasonable from a seismological point of view, we have imposed three constraints in the phase matching process. These are:

  i) A phase detection can be associated with only one hypothetical phase arrival.

  ii) A hypothetical phase arrival can be associated with only one phase detection, preferably the one with the smallest time residual.

  iii) The chronological order of the associated phase detections have to match the chronological order of the predicted phase arrivals. This is to avoid inconsistencies like an S-phase associated to arrive before a P.

  Along with the identifications of the matching detections (arids), we also store the time residuals relative to the center location of the target region. For stations providing azimuth and slowness estimates, the corresponding residuals are also stored.
- **Finding the event location from the *best* generalized beam**: If our predictions of phase arrivals are reasonable, an event should be reflected by a peak in the generalized beam representing the event target region. However, like in conventional beamforming, we encounter the problem of sidelobes, and will therefore have to select one generalized beam peak as representing the origin time and location of the event. Initially, we will use the procedure of considering the peaks at all generalized beams within a predefined time interval and select the one with the highest number of matching phases, and if equality, select the one with the smallest absolute time residual.

- **Remove associated phases and look for next event**: Once an event is located and the associated phases identified, these phases have to be removed from further consideration. This is done by recreating the generalized beams without using the phases associated to the located event, and then look for new peaks and new events.

GBF processing on a global scale with a large number of target regions is a computer intensive task. One way of reducing the computational load is to start out with a coarse grid, and then reprocess a denser grid surrounding the initial event location for a time interval around the event origin time. In the next sub-section the effect of the grid density will be illustrated with examples from GBF processing of GSETT-2 data.

The influence of grid density; an example with an earthquake in Tadjikistan

As a first test of global Generalized BeamForming, we have processed a 1 hour time interval of GSETT-2 data that included an earthquake in Tadjikistan. The event location provided by the Washington Experimental International Data Center was:

Date	Origin time	Latitude	Longitude	Depth	m_b	M_S
91/05/14	00:28:45.4	37.63N	72.30E	7 km	4.3	4.2

The GSETT-2 database consisted of detections from 60 stations, and as initial phase type candidates we used the teleseismic phases P, S and PKP, and the regional phases Pn, Pg, Sn, Lg and Rg. This is in accordance with the GSETT-2 instructions on the procedures for preparing an initial event list. Jeffereys-Bullen travel-time tables were used to predict the travel-times and slownesses, and directions along the great-circles were used to predict azimuths. Regional phases were only considered for distances within 20 degrees, and Rg only within 4 degrees. The other instructions relevant to the GBF algorithm, like time and slowness vector residual requirements and restrictions on the use of reported phases were also followed in the processing.

To investigate the influence of grid spacing on the resolution and performance of the GBF method, we first deployed a 162-point grid system covering the earth's surface. The corresponding circular areas encompassing each grid point had a radius of 11.0 degrees. For the generalized beams representing each target region, we searched for the maxima in a time interval $\pm$ 20 minutes around the origin time of the event. These maxima were then interpolated and contoured onto the global map of Fig. 7.5.8, where the color scale represents the number of associated phases at the maxima of the generalized beams. A clear peak is found at target regions near the event location, and the overall maximum was 13 associated phases.

Fig. 7.5.9 and 7.5.10 represent the same type of data, but computed with denser grid spacing. It is clearly seen that the resolution is improved and the sidelobe effect is reduced with denser grid spacing. The overall maxima in these figures were only 12 associated phases,

indicating that with a coarse grid spacing, phases with large time and/or slowness vector residuals can be associated as defining phases. However, by looking at the results from processing the coarse 162 point grid system (Fig. 7.5.8), we find that it provides a good initial location of the event. This location can subsequently be improved by constructing and processing a denser grid around the initial location.

We have in this study outlined some of the fundamentals for global Generalized Beam-Forming. The procedures for processing target regions of different areal extent has been described, and a step-by-step description of the procedure has been given. To obtain automatic event locations from processing GSETT-2 detection data, more program coding is needed. However, we have developed the framework for GBF processing on a global scale that facilitate research and testing of the method. This will become very useful in the development of the complete system.

T. Kværna

References

GSE/CRP/190/Rev.4 (1991): Instructions for the conduct of Phase 3 of GSETT-2, Group of Scientific Experts, UN Conference of Disarmament, Geneva, Switzerland.

Kværna, T. (1990): Generalized beamforming using a network of four regional arrays, Semiann. Tech. Summary, 1 April - 30 September 1990, NORSAR Sci. Rep. No. 1-90/91, Kjeller, Norway.

Kværna, T. (1992): Automatic phase association and event location using data from a network of seismic microarrays, Semiann. Tech. Summary, 1 October 1991-31 March 1992, NORSAR Sci. Rep. No. 2-91/92, Kjeller, Norway.

Ringdal, F. and T. Kværna (1989): A multi-channel processing approach to real time network detection, phase association, and threshold monitoring, Bull. Seism. Soc. Am., 79, 1927-1940.

Taylor, D.W. A. and S.K. Leonard (1992): General beamforming for automatic association, in Papers presented at the 14th Annual PL/DARPA Seismic Research Symposium, 16-18 September 1992, Loews Ventana Canyon Resort, Tucson, AZ, USA.

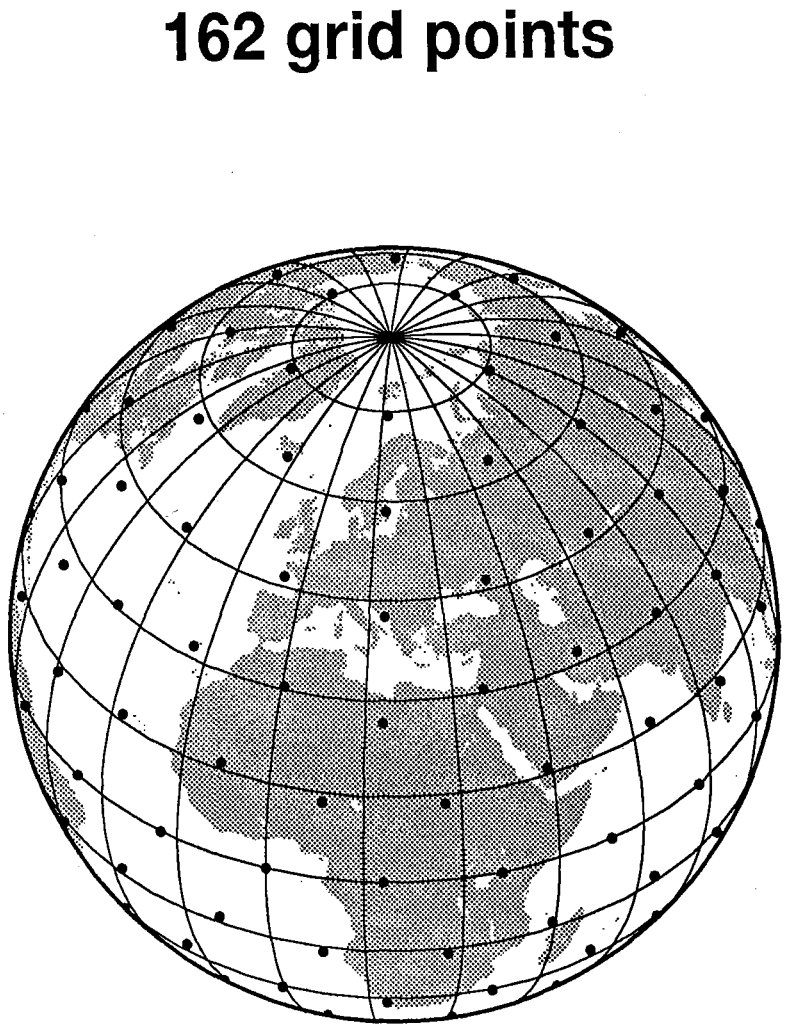

Fig. 7.5.1. A 162-point global grid system projected onto an azimutal orthographic projection of the earth. This grid system was obtained by a two-fold triangulation of the icosaeder, and each grid point represents a target region of 11 degrees radius.

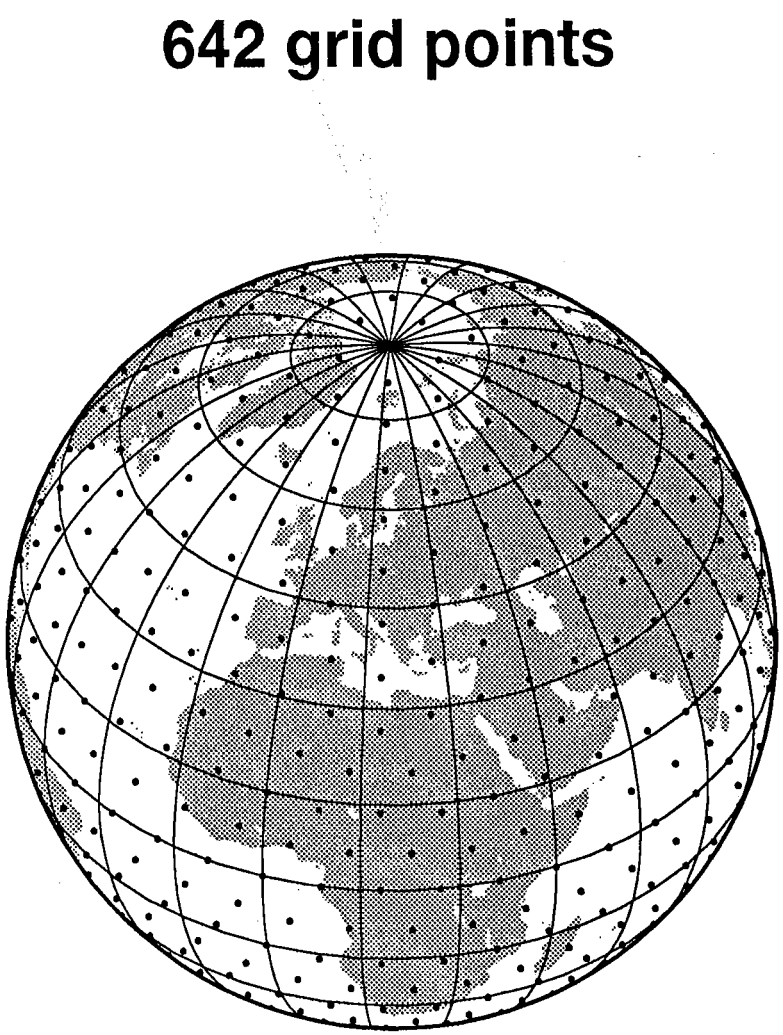

Fig. 7.5.2. A 642-point global grid system projected onto an azimutal orthographic projection of the earth. This grid system was obtained by a three-fold triangulation of the icosaeder, and each grid point represents a target region of 5.5 degrees radius.

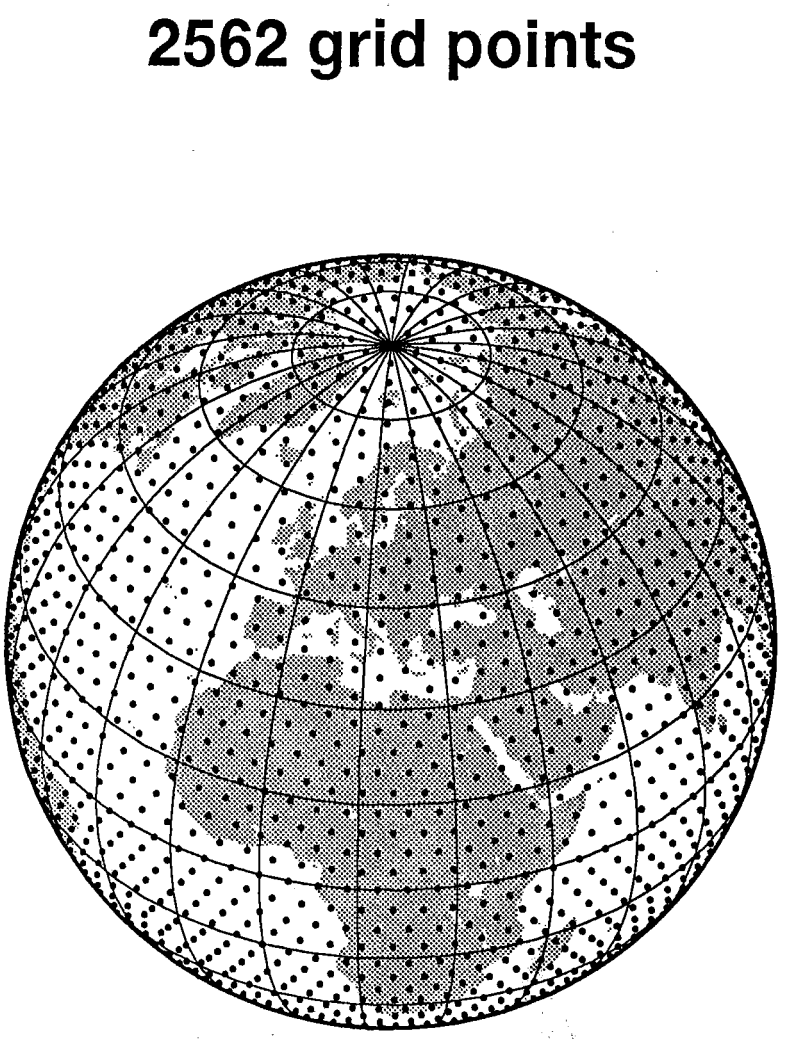

Fig. 7.5..3. A 2562-point global grid system projected onto an azimutal orthographic projection of the earth. This grid system was obtained by a four-fold triangulation of the icosaeder, and each grid point represents a target region of 2.7 degrees radius.

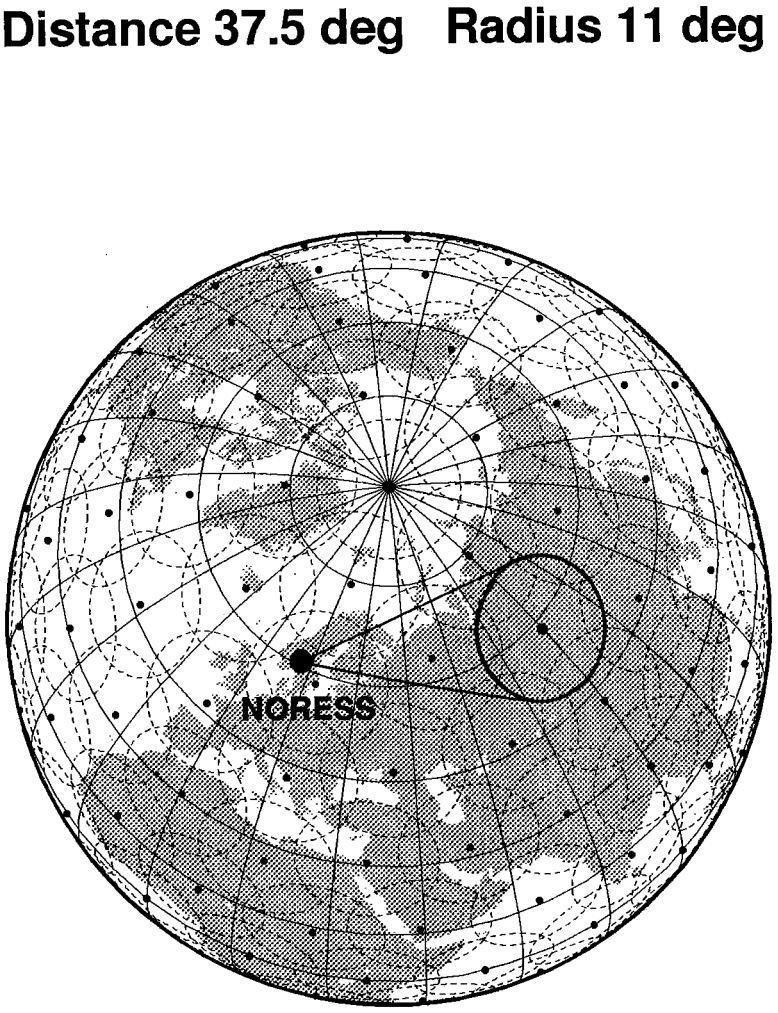

Fig. 7.5.4. A 162-point global grid system projected onto an azimutal orthographic projection of the earth. The circular target regions are shown by dashed circles, and the the highlighted target region is given special attention in this study. Its center point is located 37.5 degrees from the NORESS array. Minimum and maximum azimuthal lines from NORESS to the target region are also shown.

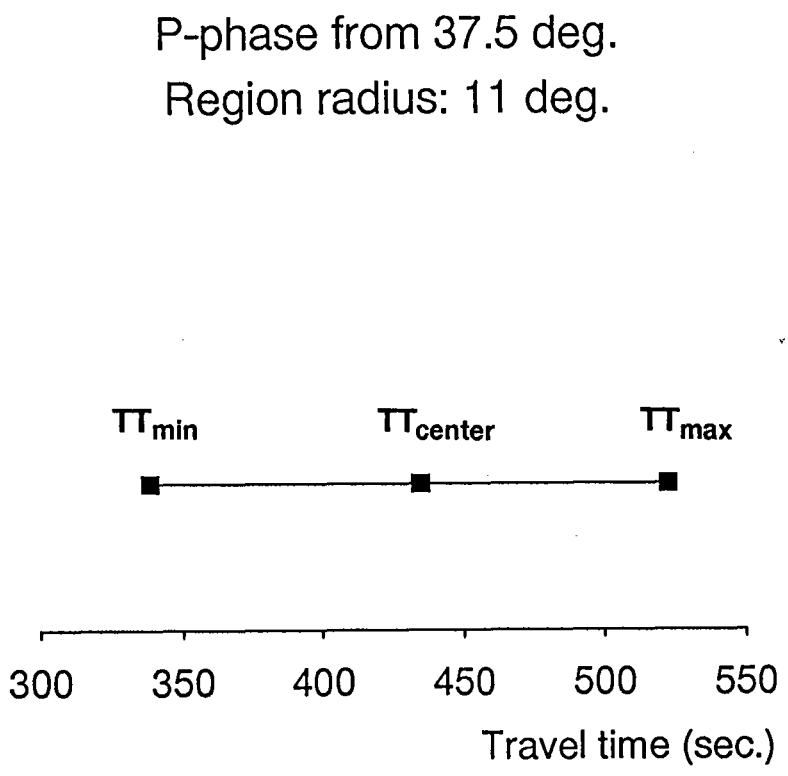

Fig. 7.5.5. Figure showing the range of predicted P-wave travel times from the highlighted target region of Fig. 7.5.4 to the NORESS array.

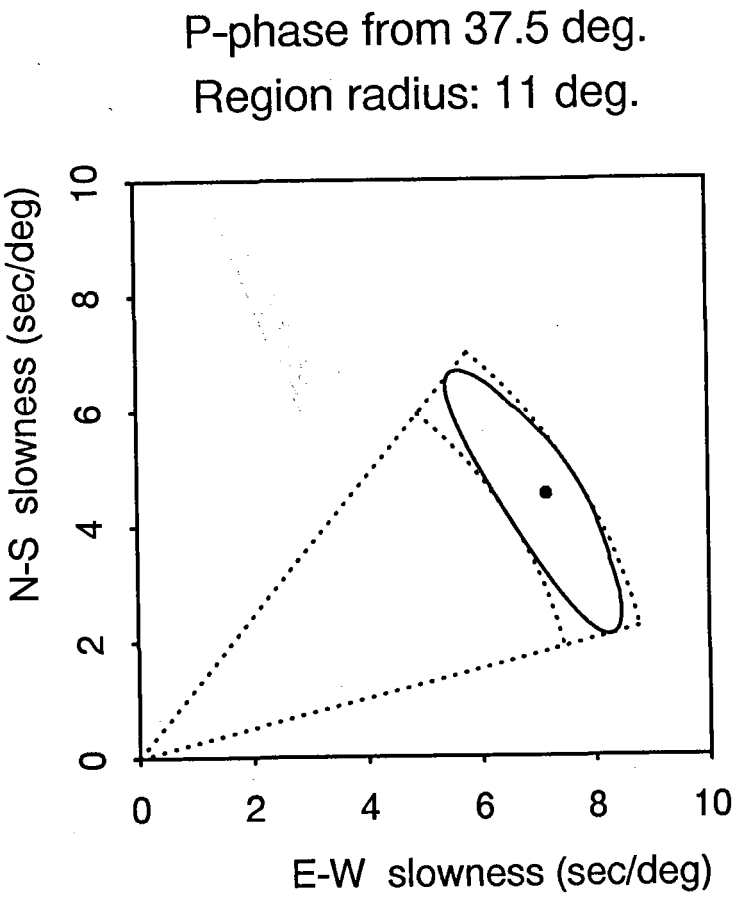

Fig. 7.5.6. Figure showing the range of predicted P-wave slowness vectors at NORESS for events in the highlighted target region of Fig. 7.5.4. The slowness vectors of the circular boundary of the target region are projeted onto the solid line of this figure. An approximation to the area inside this solid line is given by the dotted sector segment defined by the minimum and maximum azimuths and the minimum and maximum slownesses.

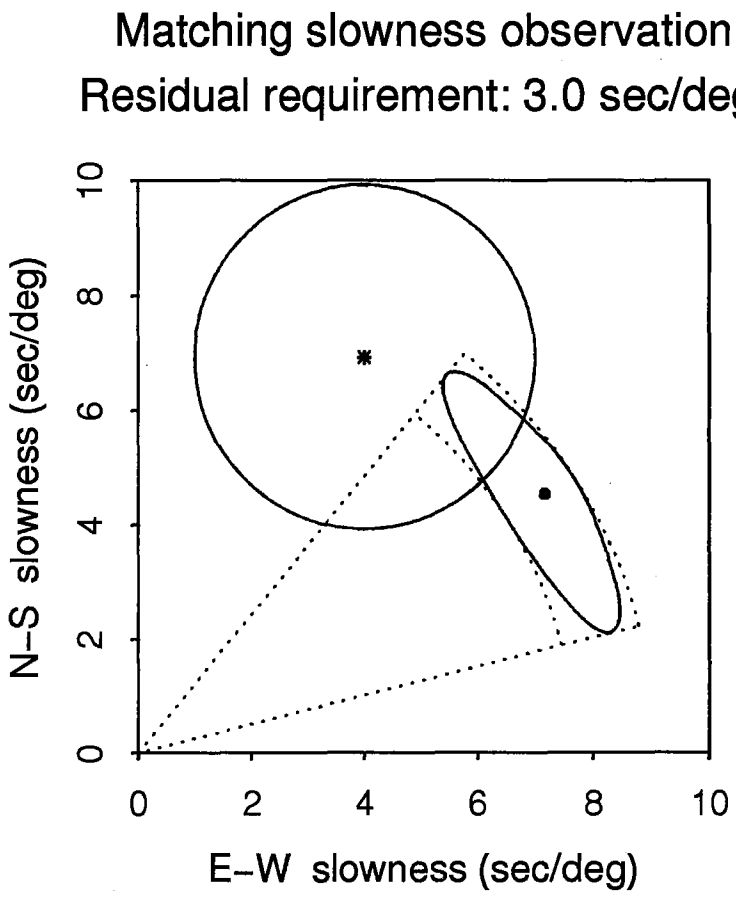

Fig.7.5.7. Figure illustrating the procedure used when matching observed and predicted slowness vectors. As explained in Fig. 7.5.6, the dotted sector segment approximate the expected range of P-wave slowness vectors for events in the target region. The slowness vector estimate of a detected phase is given by the asterisk, and the maximum allowable slowness vector residual (determined à priori) determines the surrounding circle. As seen on the figure, there is an overlap between this circular area and the sector segment corresponding to the expected range of slowness vectors for P-waves from the target region. Thereby, the phase detection is considered to match the slowness vector of the P-phase of a hypothetical event in the actual target region.

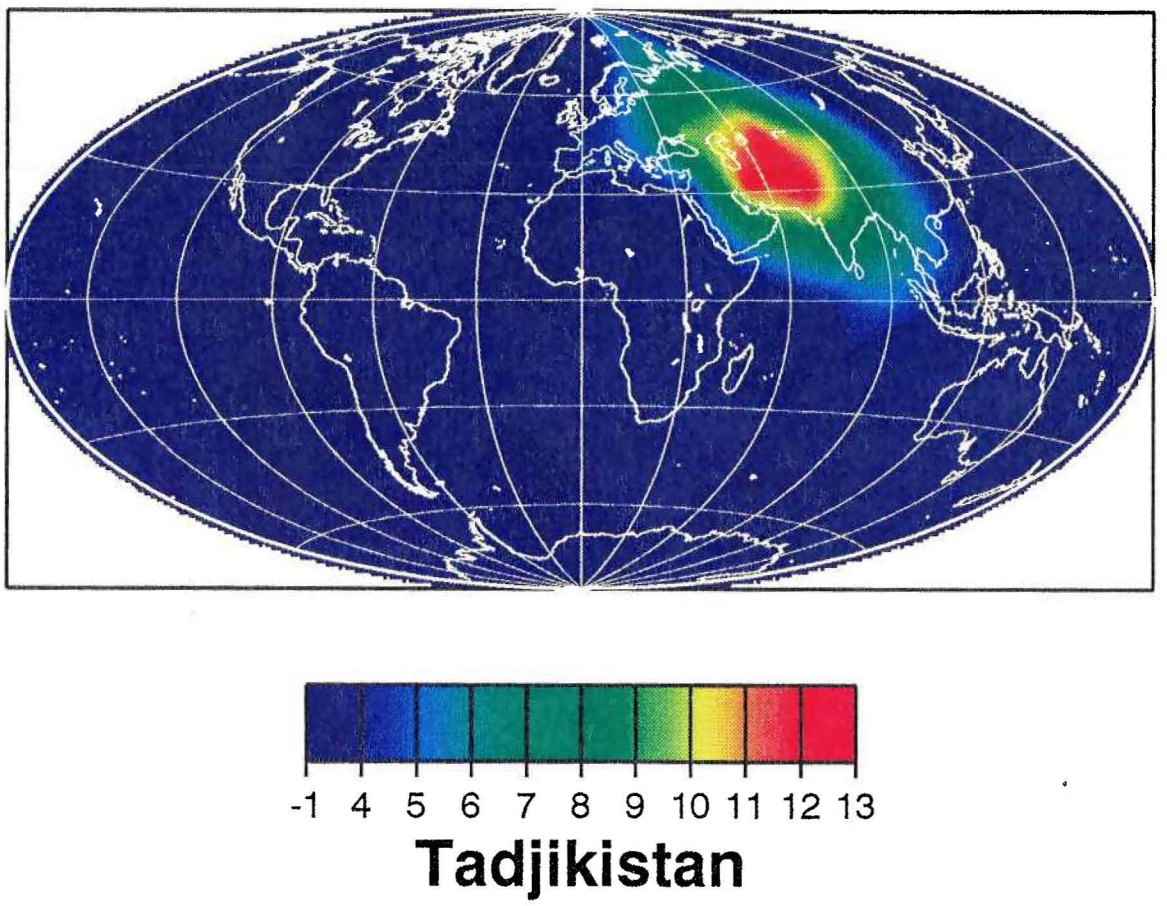

Fig. 7.5.8. Contoured maxima of generalized beams for a 162-point grid system. The maxima of each generalized beam were found by searching a time interval of ± 20 minutes around the origin time of an event in Tadjikistan. The colour scale represent the number of associated phases.

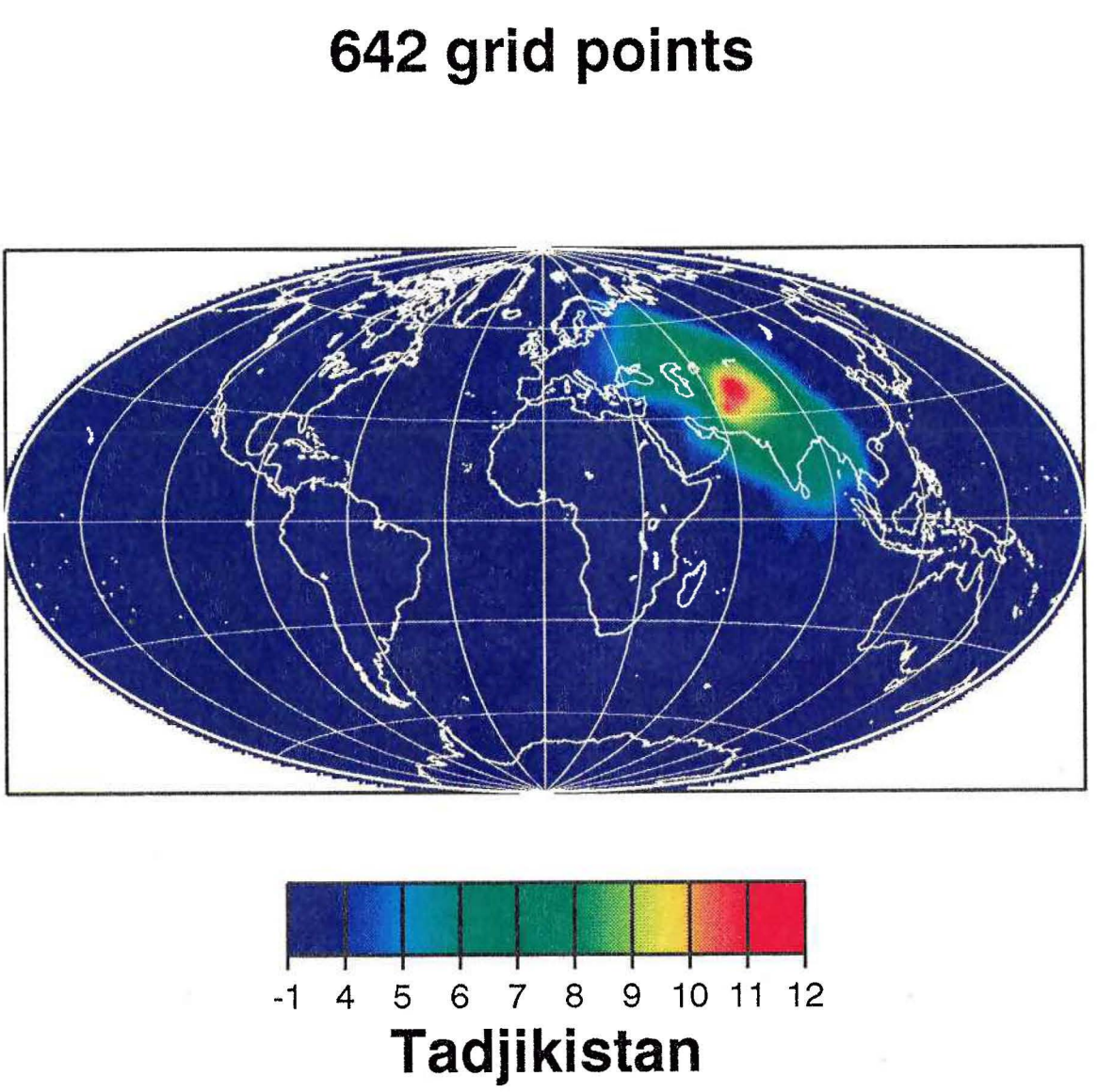

Fig. 7.5.9. Same as Fig. 7.5.8, but with a 642-point grid system.

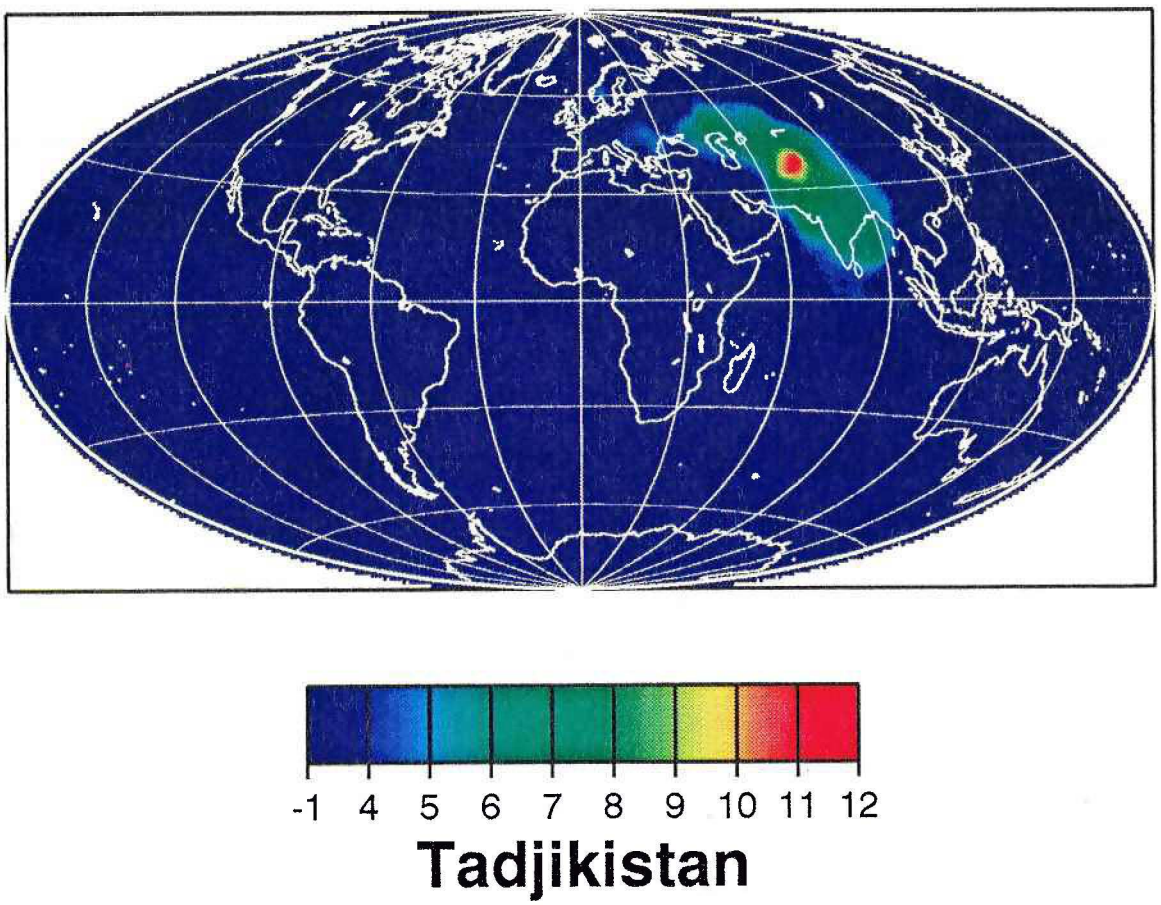

Fig. 7.5.10.. Same as Fig. 7.5.8, but with a 2562-point grid system.